Momentum distribution in vanadium: Compton scattering and positron annihilation

V. Sundararajan and D. G. Kanhere
Department of Physics, University of Poona, Pune 411 007, India

R. M. Singru
Department of Physics, Indian Institute of Technology, Kanpur 208 016, India
(Received 28 January 1992)

Self-consistent, linear-combination-of-Gaussian-orbitals band-structure method is used within the independent particle model, to calculate the electron momentum distributions, $\rho(\mathbf{p})$, and two-photon momentum distributions, $\rho^{2\gamma}(\mathbf{p})$, in metallic vanadium. We present results for $\rho(\mathbf{p})$, Compton profiles, $\rho^{2\gamma}(\mathbf{p})$, one- and two-dimensional angular correlation of positron annihilation radiation, etc. Results are compared with other calculations and with experiments wherever available. In particular, the present results for $\rho^{2\gamma}(\mathbf{p})$ are analyzed in terms of contributions from different sheets of Fermi surface of V, and are compared with $\rho^{2\gamma}(\mathbf{p})$ reconstructed from experimental two-dimensional angular correlation of positron annihilation radiation data sets by Pecora *et al.*

I. INTRODUCTION

In view of its interesting band structure and Fermi-surface (FS) topology, the electron momentum distribution in metallic V has been well studied theoretically, using different methods of band structure, and experimentally, using the Compton scattering and positron annihilation techniques. While the electron momentum distribution $\rho(\mathbf{p})$ is the quantity studied in Compton scattering,[1] the positron annihilation technique[2] probes the two-photon momentum distribution $\rho^{2\gamma}(\mathbf{p})$. Such theoretical studies of V have used the Korringa-Kohn-Rostoker,[3] augmented-plane wave (APW),[4–7] Hubbard's fast approximate scheme,[8] linear muffin-tin orbital,[9–11] and linear-combination-of-atomic-orbitals (Ref. 12) methods of band structure while the experimental measurements have been carried out by using x-ray,[13] γ-ray,[14–18] and synchrotron radiation[19] Compton scattering, as well as one-dimensional[20] (1D) and two-dimensional[21,22] angular correlation of positron annihilation radiation (ACAR) studies. Recent technical developments[23] have now made it possible to measure the Compton profiles

$$J(p_z)=\int\int_{-\infty}^{+\infty}\rho(\mathbf{p})dp_x dp_y \tag{1}$$

with high-momentum resolution ($\sim$0.1 a.u.) which is as good as that available in some ACAR measurements. The 2D ACAR experiment offers 2D data sets

$$N(p_y,p_z)=\int_{-\infty}^{+\infty}\rho^{2\gamma}(\mathbf{p})dp_x \tag{2}$$

and it allows an easier reconstruction[24] of $\rho^{2\gamma}(\mathbf{p})$ from the measured data sets $N(p_y,p_z)$. The theoretical calculations of $\rho(\mathbf{p})$ and $\rho^{2\gamma}(\mathbf{p})$ are usually carried out in the independent particle model and for a more complete description it is necessary to include e^--e^- correlations[1] for $\rho(\mathbf{p})$ and positron wave functions[25] as well as e^+-e^- many-body correlations[25] for $\rho^{2\gamma}(\mathbf{p})$. It is well known[26,27] that the effect of e^--e^- correlations on $\rho(\mathbf{p})$ is to raise some electrons from levels just below ($p<p_F$) the FS to levels just above ($p>p_F$) it without shifting the discontinuity at $p=p_F$, which marks the FS. Introduction of a positron as a probe in a metal introduces the effects of positron wave function[25] and e^+-e^- many-body correlations[25] and this renders the shape of $\rho^{2\gamma}(\mathbf{p})$ different from that of $\rho(\mathbf{p})$, although the discontinuities due to FS still occur at $p=p_F$.[28] The information about the FS can thus be obtained from $\rho(\mathbf{p})$ and $\rho^{2\gamma}(\mathbf{p})$ in a complementary way. Although the effects of positron wave function on $\rho^{2\gamma}(\mathbf{p})$ were known[25] for some time, good progress in calculating the effects of e^--e^- correlations[7,29,30] on $\rho(p)$ and e^+-e^- many-body correlations[31–34] on $\rho^{2\gamma}(\mathbf{p})$ in 3d transition metals has been made only recently. For a systematic understanding of these effects it is desirable that the band theoretical calculations of $\rho(\mathbf{p})$ and $\rho^{2\gamma}(\mathbf{p})$ be carried out using the same set of electron wave functions and the same band-structure methods. Keeping this in mind, we have calculated $\rho(\mathbf{p})$ and $\rho^{2\gamma}(\mathbf{p})$ in metallic V using the same set of electron wave functions and the linear-combination-of-Gaussian-orbitals (LCGO) method, which is known to describe the experimental data of CP in V satisfactorily.[17,18] Although Laurent, Wang, and Callaway[12] have calculated the CP in V using the LCGO method, we have incorporated two improvements in the present work: (i) the treatment of exchange and correlation potential was improved. Cardwell and Cooper[35] have compared the results for Compton profiles calculated by the APW and LCGO methods for V, Cr, Ni, and Fe and have concluded that a proper formulation of exchange and correlation in the LCGO theory is important; (ii) the LCGO method[12] has been extended[36] to calculate $\rho^{2\gamma}(\mathbf{p})$ and ACAR distributions $N(p_y,p_z)$. The results of the present calculations are compared with experiment, in particular, with the high-resolution Compton profile data measured with synchrotron x rays[19] and $\rho^{2\gamma}(\mathbf{p})$ reconstructed from the measured 2D ACAR data sets.[22,37]

II. CALCULATIONAL PROCEDURE

The distributions $\rho(\mathbf{p})$ and $\rho^{2\gamma}(\mathbf{p})$ in V were calculated using the LCGO method described elsewhere.[36,38] The LCGO method carries certain advantages, such as its self-consistent character and the absence of any shape-dependent approximation. Another advantage relevant here is that the Gaussian nature of the basis functions in the LCGO method allows one to compute the $\rho(\mathbf{p})$ and $\rho^{2\gamma}(\mathbf{p})$ up to a desired high-momentum (p) value analytically and accurately and this is an important advantage while obtaining Compton profile (or ACAR) curves from the integration involved in Eqs. (1) and (2) in the p space. Our previous application of this extended version of the LCGO method to Fe, Ni, and Cu has already provided satisfactory results.[36]

In the present calculations, the Gaussian basis set consisting of thirteen s, ten p, five d, and one f functions and the lattice constant $a=5.7445$ a.u. were used. The previous LCGO calculation by Laurent, Wang, and Callaway[12] used the exchange-only approximation while the present work used the exchange-correlation potential of von Barth and Hedin as parametrized by Rajagopal, Singhal, and Kimball.[39] The positron wave function having Γ_1 symmetry was also calculated under the framework of LCGO theory using seven s Gaussian orbitals by reversing the sign of the electron potential and removing the exchange part. Contribution to $\rho(\mathbf{p})$ due to the band electrons was calculated up to $p=10.0$ a.u. using a total of 2123 reciprocal-lattice vectors and it yielded a value of 4.99 electrons, thus indicating the high accuracy achieved. A total of 135 reciprocal-lattice vectors were used to compute $\rho^{2\gamma}(\mathbf{p})$ up to $p=4.0$ a.u. These computations were performed in the independent-particle model with no corrections made for the e^--e^- or e^+-e^- correlations in the first stage.

III. RESULTS AND DISCUSSION

A. Electron momentum distributions and Compton profiles

As a typical result of the present calculation, we have plotted in Fig. 1 $\rho(\mathbf{p})$ in the form of the surface $\rho(p_x,p_y,p_z=0)$ in the plane $(p_x,p_y)=(100)$. The overall shape of this surface is determined by the electron wave functions while the sharp structures observed in Fig. 1 arise out of the FS topology. It is well known that the FS of V (see Figs. 3 and 4 of Ref. 12) shows the following features: (i) second-band octahedral hole surface centered at Γ, (ii) third-band distorted ellipsoidal hole surface centered at N, and (iii) third-band multiply connected arms along the $\langle 100 \rangle$ directions. The structures seen in Fig. 1 can be more readily understood by referring to Fig. 2 of Ref. 40, where the FS of V in the (010) plane is shown in the extended-zone scheme. Thus, for example, the craterlike depression seen at $p_x=0.5(2\pi/a)$, $p_y=0.5(2\pi/a)$, and $p_z=0$ reflects the effect of the third-band N-centered ellipsoidal hole and its Umklapp image is also seen, with reduced amplitude, further along the [110] direction. Another minor depression having a square shape is centered around $p_x=2\pi/a, p_y=2\pi/a$ and has its edges parallel to the Brillouin zone boundaries. It is ascribed to the combined effect of the second-band Γ-centered octahedral hole and third-band jungle-gym arms. It is now recognized that theoretical results for the surfaces (e.g., Fig. 1) and contours of $\rho(\mathbf{p})$ in different (p_x,p_y) planes can provide a basis with which to compare similar distributions obtained by the reconstruction of $\rho(\mathbf{p})$ from a set of Compton profiles measured for several directions. Such a reconstruction effort for Fe using 14 magnetic Compton profiles has been recently reported by Sakai.[41] At this point a comment about the previous effort by Das, Bhagwat, and Sahni[42] to reconstruct electron momentum distributions in V using experimental Compton profiles might be in order. These authors applied the method of Radon transform to reconstruct $\rho(\mathbf{p})$ from a set of three directional Compton profiles measured for V for the [100], [110], and [111] directions. Their results indicated that the shapes of $\rho(\mathbf{p})$ along the $p=$[100], [110], and [111] in V are almost similar and they show monotonically decreasing behavior devoid of any structures. However, the present results (Fig. 1) and the previous reports[8,9,37] clearly show that $\rho(\mathbf{p})$ in V has strong discontinuities along the [110] and [111] directions that survive the smearing effect brought on by the reconstruction scheme.[37] We attribute this discrepancy to the fact that the reconstruction effort of Das, Bhagwat, and Sahni[42] was incomplete because they used only three directional Compton profiles, and thus their expansion of $\rho(\mathbf{p})$ in terms of three kubic harmonics (K_0, K_1, and K_2) had perhaps not converged fully. In view of the anisotropy and sharp discontinuities present in the $\rho(\mathbf{p})$ of V, many more directional Compton profiles will have to be used to ensure a nearly complete reconstruction of $\rho(\mathbf{p})$ in V.

Recently, Shiotani *et al.*[19] have measured the Compton profiles for V along the [100] direction with an overall momentum resolution of 0.12 a.u. using 59.38-keV x rays from synchrotron. A comparison of their experimental results with the APW theory[7] has shown that

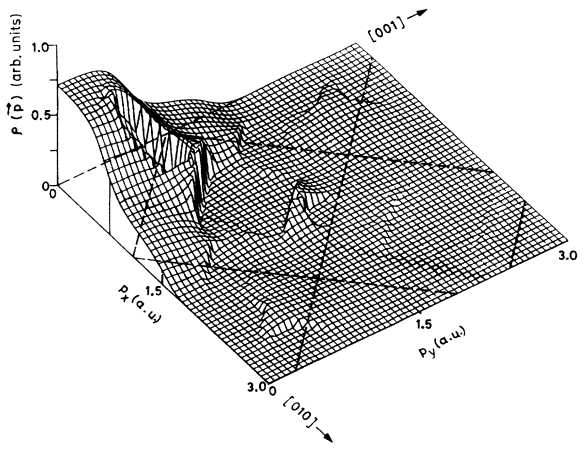

FIG. 1. Plot of $\rho(p_x,p_y,p_z=0)$ for V in the plane $(p_x,p_y)=(100)$ passing through the point Γ.

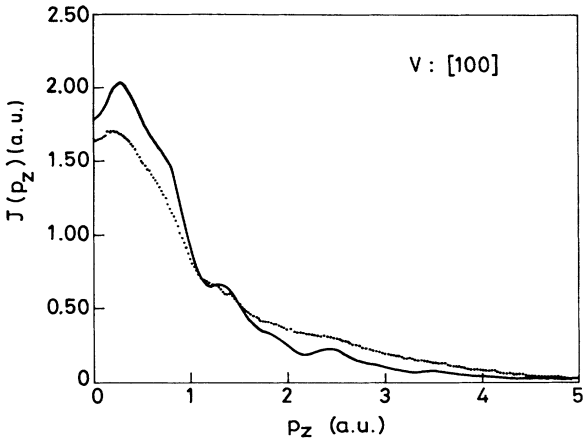

FIG. 2. Comparison of the present theoretical (LCGO) Compton profile (solid curve) for the band electrons of V along the [100] direction with experimental[19] CP (dotted curve). The theoretical curve is convoluted with a Gaussian of full width at half maximum (FWHM)=0.12 a.u.

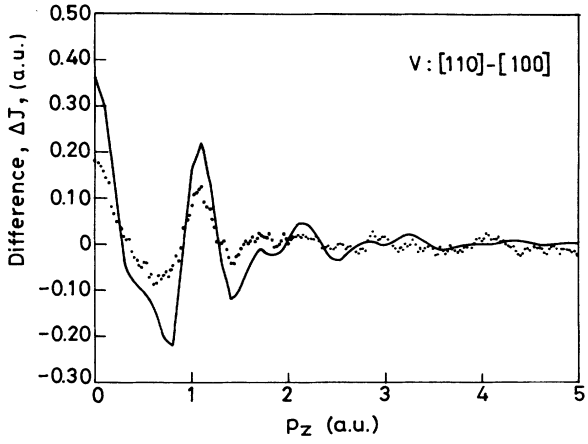

FIG. 3. Comparison of the present theoretical (LCGO) difference Compton profile, ΔJ (solid curve) for V for the ([110]-[100]) directions with experimental[19] ΔJ curve (dotted curve). The theoretical curve is convoluted with a Gaussian of FWHM=0.12 a.u.

there is good agreement in the characteristic features of the two profiles, with the structure appearing sharper in the theoretical curve. In its overall shape, the APW theory overestimates the Compton profile $J(p_z)$ in the low ($p_z < 1$ a.u.) -momentum region but underestimates it in the high ($p_z > 1$ a.u.) -momentum region. The theoretical (LCGO) Compton profile calculated by us for the band electrons of V (Fig. 2) shows an excellent agreement with the APW theory as presented by Shiotani *et al.*[19] Thus, the two theories (APW and LCGO) agree closely among themselves but both predict Compton profiles that are higher than experiment [$\sim 8\%$ $J(0)$ at $p_z=0$] at low ($p_z < 1.0$ a.u.) momenta and lower at high ($p_z > 1.0$ a.u.) momenta (Fig. 2). The concavity in $J(p_z)$ at $p_z=0$ and $p_z=(2\pi/a)$ has been explained in terms of the FS topology earlier.[3,4,6,17,18] The anisotropy or difference profile $\Delta J=(J_{110}-J_{100})$ calculated by us is shown in Fig. 3 where it is compared with experiment. We have observed that the LCGO theoretical curve (Fig. 3) agrees very closely with the APW theory (not shown here but reported in Ref. 19). However, both the theories display larger amplitudes of the oscillation in the ΔJ curve, although the general trend of theoretical and experimental curves is similar. The same observation was made when we compared the present theoretical ΔJ curves with those measured by Rollason and co-workers[17,18] with poorer (0.39 a.u.) resolution using γ rays. Such discrepancies between theory and experiment have also been observed for other transition metals.[1] The present results confirm, once again, that the source of these discrepancies lies not in a particular band theory but in the nature of the independent particle model used. As pointed out earlier,[43,44] a solution to the problem can be found by including the e^--e^- correlation effects. To test this point we applied the Lam-Platzman correction[45] to our LCGO results for $J(p_z)$. Although this procedure helped to bring down the differences between present theory and experiment, the theory still overestimated experiment in the low-momentum region and the residual differences appeared anisotropic, thus proving the inadequacy of the Lam-Platzman correction, which is isotropic. Recent work by Cardwell, Cooper, and Wakoh[29] on Cr and by Wakoh and Matsumoto[7] on V and Cr has indicated how the anisotropic e^--e^- correlation effects can be calculated. In particular, the latter study[7] has shown that in the case of V the effects of e^--e^- correlation on $\rho(\mathbf{p})$ are determined by the energy occupation function for the d bands. We plan to incorporate such corrections in our LCGO scheme in the future. Until then, the present results indicate that the LCGO theory provides a good basis to calculate $\rho(\mathbf{p})$ in V using the independent particle model.

B. Two-photon momentum distributions

After having tested the quality of the one-electron wave functions used by us, we proceeded to calculate $\rho^{2\gamma}(\mathbf{p})$ and ACAR distributions in V. With the present results, the interest in the theoretical $\rho^{2\gamma}(\mathbf{p})$ is twofold: (i) first it can be used to compute 2D and 1D ACAR distributions, which can be compared with experiment; (ii) second, the theoretical $\rho^{2\gamma}(\mathbf{p})$ can be compared, through its surfaces and contours, with the $\rho^{2\gamma}(\mathbf{p})$ reconstructed from experimental 2D ACAR data sets. The former method is more useful for providing quantitative information about the e^+-e^- many-body correlation corrections needed, while the latter method can be used to examine the FS topology.

Recently Pecora *et al.*[37] have reconstructed $\rho^{2\gamma}(\mathbf{p})$ in V using the high-resolution 2D ACAR data sets measured for four crystalline orientations.[21] In their work, a direct comparison has been made between the $\rho^{2\gamma}(\mathbf{p})$ reconstructed from the experimental[21] and theoretical[40] 2D ACAR data sets. In view of the merits of the LCGO theory used by us, we have compared (Figs. 4–6) the ex-

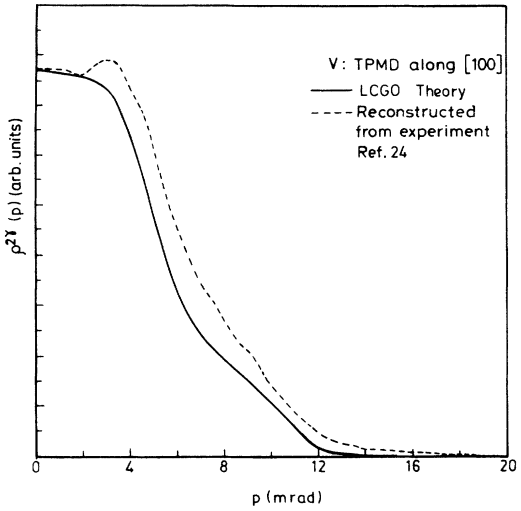

FIG. 4. Present theoretical (LCGO) $\rho^{2\gamma}(\mathbf{p})$ (solid curve) compared with $\rho^{2\gamma}(\mathbf{p})$ reconstructed from experiment[37] (dashed curve) along the [100] direction in V. Relevant band structure is shown in Ref. 37.

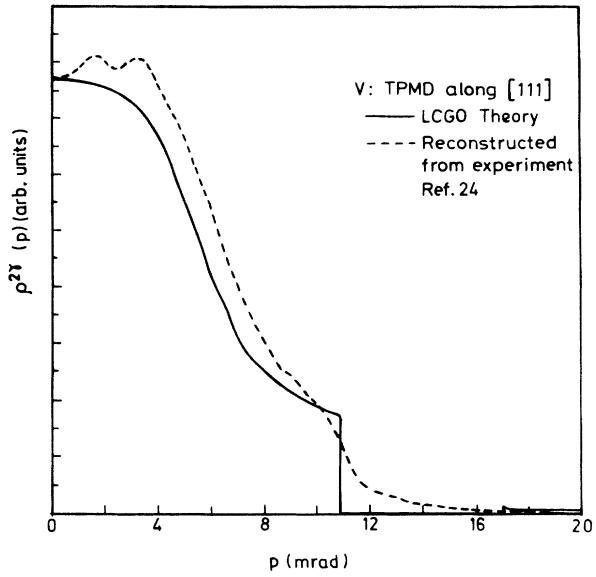

FIG. 6. Same as Fig. 5 but for the [111] direction.

perimental $\rho^{2\gamma}(\mathbf{p})$ reconstructed by Pecora *et al.*[37] with $\rho^{2\gamma}(\mathbf{p})$ calculated by us. It is observed that theory and experiment show similar trends, with the theoretical curves showing sharper FS breaks along the [110] and [111] directions. Particular attention is drawn to the interesting structure in the $\rho^{2\gamma}(\mathbf{p})$ curve along the [110] direction (Fig. 5). Theoretical curves show a "spike" at $p \sim 0.45$ a.u. or 3.3 mrad (and its Umklapp images), which arises from the dipping of the second $\sum_1$ band below the Fermi level by a few mRy between Γ and N.[12,21,40] The comparison shown in Fig. 5 once again confirms that such a dipping of the second $\sum_1$ band exists and that there is no

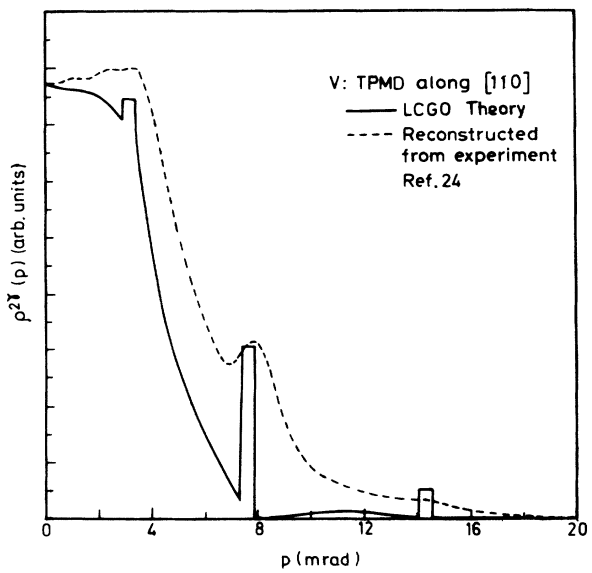

FIG. 5. Same as Fig. 4 but for the [110] direction.

neck along ΓN in the FS of V. Following Pecora *et al.*,[37] the slight shift of FS breaks observed in Figs. 5 and 6 can be attributed to the small difference in the experimental lattice parameter and the value used in our calculations. Possible factors responsible for the differences between theory and experiment (as seen in Figs. 4–6) have been pointed out by Pecora *et al.*[37] However, we wish to underline one important feature. Present results as shown in Figs. 4–6 might suggest that the present theory (in the independent particle model) underestimates experiment. It should, however, be remembered that we have normalized both the $\rho^{2\gamma}(\mathbf{p})$ curves at $p=0$ for each direction. This might not be a correct procedure to follow because it has been proposed[33,34,46,47] that the two-photon momentum distribution $\rho^{\text{enh}}_{\mathbf{k},j}(\mathbf{p})$, enhanced by the e^+-e^- many-body correlations, is related to $\rho^{2\gamma}_{\mathbf{k},j}(\mathbf{p})$, calculated in the independent particle model, through the relation

$$\rho^{\text{enh}}_{\mathbf{k},j}(\mathbf{p}) = \epsilon_{\mathbf{k},j}(E)\rho^{2\gamma}_{\mathbf{k},j}(\mathbf{p}) , \tag{3}$$

where $\mathbf{k}$ denotes the wave vector and j the band index of the electron and $\epsilon_{\mathbf{k},j}(E)$ is the enhancement factor, which might be character or state dependent.[34] Thus, $\epsilon_{\mathbf{k},j}(E)$ might not be 1 at $p=0$ and, in that case, a different normalization between theory and experiment will have to be followed. It is difficult to determine the normalization without knowing the quantitative treatment of the e^+-e^- many-body correlation correction. As an aid to the understanding of the effect of positron wave function, we give in Table I the ratios of the weighted areas of pure s, p, and d contributions to $\rho(\mathbf{p})$ and $\rho^{2\gamma}(\mathbf{p})$ in V. In view of the uncertainty about the e^+-e^- many-body correlation corrections, it might be more useful to carry out the comparison between experiment and theory in terms of the contours of $\rho^{2\gamma}(\mathbf{p})$ in the (p_y,p_z) planes. Accordingly, we have shown in Figs. 7 and 8 the contour plots of $\rho^{2\gamma}(\mathbf{p})$

TABLE I. The ratio of the weighted areas of pure s, p, and d contributions to the total $\rho(\mathbf{p})$ and $\rho^{2\gamma}(\mathbf{p})$ in V.

Direction \ State	s		p		d	
	$\rho(\mathbf{p})$	$\rho^{2\gamma}(\mathbf{p})$	$\rho(\mathbf{p})$	$\rho^{2\gamma}(\mathbf{p})$	$\rho(\mathbf{p})$	$\rho^{2\gamma}(\mathbf{p})$
⟨100⟩	0.095	0.088	0.143	0.141	0.707	0.581
⟨110⟩	0.288	0.471	0.089	0.090	0.637	0.363
⟨111⟩	0.046	0.084	0.095	0.135	0.512	0.344

calculated by us in the (100) and (110) planes, respectively. The effect of the FS topology of V is seen clearly in these contour plots. Thus, the four ellipsoidal pockets observed in Fig. 7 at $p_y=\pm 0.5(2\pi/a)$ and $p_z=\pm 0.5(2\pi/a)$ and the two pockets observed in Fig. 8 at $p_y=\pm(1/\sqrt{2})(2\pi/a)$ and $p_z=0$ arise out of the N-centered elipsoidal holes. Recently, Kubota *et al.*[22] have measured 2D ACAR spectra from V single crystals for ten orientations and have reconstructed $\rho^{2\gamma}(\mathbf{p})$ from these data sets. Their results for the contour plots in the plane $(p_y,p_z)=(100)$, $p_x=0$ (not shown here) show a striking agreement with the present theory (Fig. 7). These results indicate that within the independent particle model the LCGO theory can provide a satisfactory basis with which to calculate $\rho^{2\gamma}(\mathbf{p})$ in V in the first stage.

We shall now show the 1D and 2D ACAR curves calculated from the present results for $\rho^{2\gamma}(\mathbf{p})$. The 1D ACAR curves are shown in the form of difference curves in Fig. 9, where they are compared with the experiment.[20] Such a comparison shows that best agreement is obtained for the ([110]-[100]) directions, fair agreement for the ([111]-[100]) directions and rather poor agreement for the ([111]-[110]) directions. Similar behavior was observed when the same 1D ACAR data were compared with the APW theory.[4] The discrepancies observed in Fig. 9 are thus caused not by any particular band theory

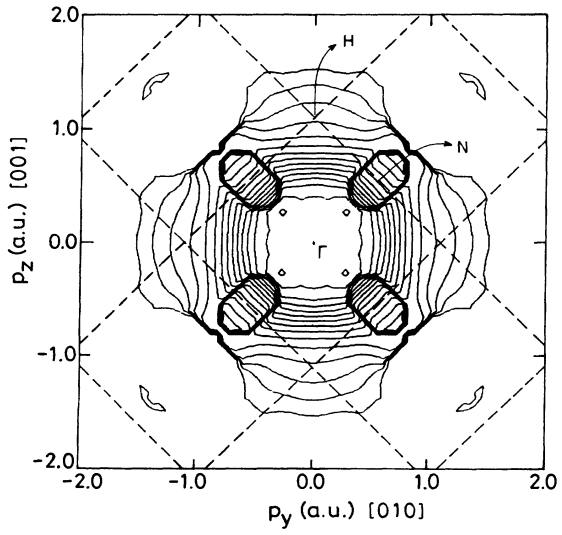

FIG. 7. Contour plot of the present theoretical (LCGO) $\rho^{2\gamma}(\mathbf{p})$, in the (100) plane.

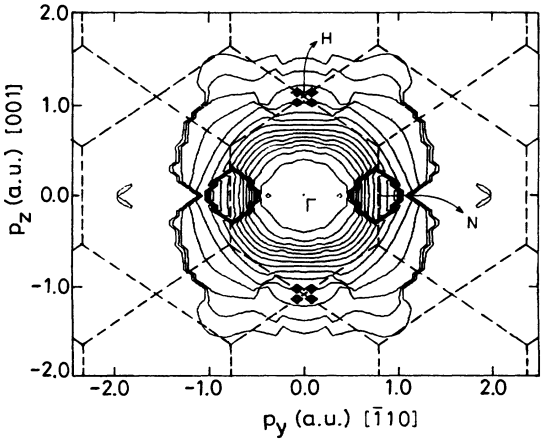

FIG. 8. Same as Fig. 7 but for the (110) plane.

but by the limitations of the independent particle model (i.e., neglect of e^+-e^- many-body correlation effects). The characteristic structures observed in Fig. 9 have been explained in terms of the FS topology in the literature.[4,20] The present results for the 2D ACAR single curves $N(p_y,p_z)$ along the two lines for the orientation $p_x=[110]$ are (A) $N\{\vec{p}_y=(0,0,0),\ \vec{p}_z\ \|[001]\}$ and (B) $N\{\vec{p}_y\|\ [\bar{1}10],\ \vec{p}_z=(0,0,0)\}$ are shown in Fig. 10, where they are compared with the experimental results reported by Singh *et al.*[21] Concavity observed in curve A at $p=0$, and $p=2\pi/a$ and in curve B at $p=0$, $p=(2\pi/a)/\sqrt{2}$, and $p=2(2\pi/a)/\sqrt{2}$ are caused by the third-band FS (N-centered ellipsoidal hole and multiply connected arms)

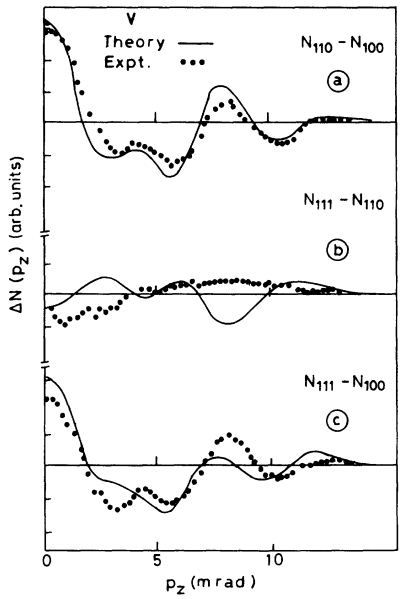

FIG. 9. Difference (curves) $\Delta N=(N_{hkl}-N_{h'k'l'})$ for V for (a) ([110]-[100]), (b) ([111]-[110]), and (c) ([111]-[100]) directions. The solid curve represents LCGO theory while the solid circles represent experimental data.[20]

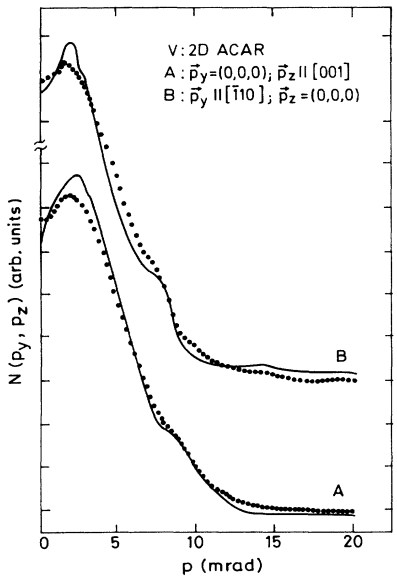

FIG. 10. Comparison of the present theoretical (LCGO) and experimental[21] 2D ACAR curves along two lines for the orientation [110]: (*A*) $N\{\vec{p}_y=(0,0,0),\vec{p}_z\|$ [001] } and (*B*) $N\{\vec{p}_y\|[\bar{1}10]$, $\vec{p}_z=(0,0,0)\}$. Solid curves denote theory while solid circles represent experimental points.

of V. While comparing the present theory with experiment (Fig. 10) it should be remembered that the core-electron contribution to the theoretical 2D ACAR curve was not reduced by any factor. Similarly, no enhancement correction for the e^+-e^- many-body correlation was applied. Closer agreement between theory and experiment was obtained by Genoud[10] after applying these two corrections. We feel that the neglect of these two corrections in the present work is responsible for the differences between theory and experiment observed in Fig. 10. However, these two corrections could not be determined without the availability of complete numerical data from the 2D ACAR experiment and, hence, we have left the comparison in the form shown in Fig. 10.

Kubota *et al.*[22] have determined the dimensions of the FS of V from the analysis of their 2D ACAR experiment. The values obtained by them are compared with the present LCGO theory in Table II. It is observed that the dimensions of the third-band and *N*-centered ellipsoidal hole (along $N\Gamma$ and *NH*) as obtained from the experiment are lower than theoretical predictions. Similar observation has been made for V earlier.[21,48] There is satisfactory agreement between theory and experiment for other

TABLE II. A comparison of the dimensions of the FS of V obtained by experiment (Ref. 22) and present theory. All values are in a.u. NCE: third-band *N*-centered ellipsoids. GCO: second-band Γ-centered octahedra. MCA: third-band multiply connected arms.

	$\Gamma\rightarrow N$	$N\rightarrow\Gamma$ NCE	$N\rightarrow H$ NCE	$\Gamma\rightarrow H$ GCO	$H\rightarrow N$ MCA
Experiment (Ref. 22)	0.31 ±0.02	0.17 ±0.02	0.12 ±0.02	0.38 ±0.02	0.40 ±0.02
Present theory	GCO 0.24 MCA 0.35	0.28	0.18	0.44	0.43

FS dimensions (Table II). It is usual to compare theoretical $\rho^{2\gamma}(\mathbf{p})$ with experiment by plotting (i) **k**-space momentum distributions using the Lock-Crisp-West folding[49] and (ii) the Fourier transform of momentum density or the autocorrelation function $B^{2\gamma}(\mathbf{r})$.[2] We have calculated these functions from our theory and they show satisfactory agreement with experiment[50] and other theory.[40,50] These results are not shown here for lack of space, but they can be made available on request.

IV. CONCLUSIONS

Self-consistent band calculations of the electron and two-photon momentum distribution in metallic V have been made in the independent particle model using the LCGO method. Directional Compton profiles and 1D and 2D ACAR curves have also been calculated. The present theoretical Compton profile curve agrees very well with the results of APW calculations and both theories show the same differences with experiment which are attributed to the e^--e^- correlations. Present theoretical results for the 1D and 2D ACAR are compared with experiment and the residual differences are attributed to the e^+-e^- many-body correlations. On the whole, the LCGO theory is found to give satisfactory description of the momentum distributions in V.

ACKNOWLEDGMENTS

This work was supported by the Department of Atomic Energy, Government of India and Department of Science and Technology (Grant No. SP/S2/M-39/87), Government of India. We are grateful to Dr. N. Shiotani, Dr. N. Sakai, and Dr. S. Tanigawa for sending us their results prior to publication.

[1]M. Cooper, Rep. Prog. Phys. **48**, 415 (1985).

[2]S. Berko in *Positron Solid-State Physics,* edited by W. Brandt and A. Dupasquier (North-Holland, Amsterdam, 1983), p. 64.

[3]S. Wakoh and J. Yamashita, J. Phys. Soc. Jpn. **35**, 1406 (1973).

[4]S. Wakoh, Y. Kubo, and J. Yamashita, J. Phys. Soc. Jpn. **40**, 1043 (1976); *ibid.* **38**, 416 (1975).

[5]M. Matsumoto and S. Wakoh, J. Phys. Soc. Jpn. **55**, 3948 (1986).

[6]N. I. Papanicolaou, N. C. Bacalis, and D. A. Papaconstantopoulos, Z. Phys. B **65**, 453 (1987).

[7]S. Wakoh and M. Matsumoto, J. Phys. Condens. Matter **2**, 797 (1990).

[8]D. G. Kanhere and R. M. Singru, J. Phys. F **7**, 2603 (1977).
[9]A. K. Singh and T. Jarlborg, J. Phys. F **15**, 727 (1985).
[10]P. Genoud, Ph.D. thesis, University of Geneva, 1990; see also A. A. Manuel, A. K. Singh, T. Jarlborg, P. Genoud, L. Hoffmann, and M. Peter, in *Positron Annihilation,* edited by L. Dorikens-Vanpraet, M. Dorikens, and D. Segers (World Scientific, Singapore, 1989), p. 109.
[11]M. Heilper, J. Ashkenazi, and J. Felsteiner, Phys. Rev. B **33**, 755 (1986).
[12]D. G. Laurent, C. S. Wang, and J. Callaway, Phys. Rev. B **17**, 455 (1978).
[13]W. C. Phillips, Phys. Rev. B **7**, 1047 (1973).
[14]O. Terasaki, T. Fukamachi, S. Hosoya, and D. Watanabe, Phys. Lett. **43A**, 123 (1973).
[15]T. Paakkari, P. Suortti, V. Halonen, and S. Manninen, Phys. Fenn. **8**, 93 (1973).
[16]F. Itoh, T. Honda, H. Asano, M. Hirabayashi, and K. Suzuki, J. Phys. Soc. Jpn. **49**, 202 (1980).
[17]A. Rollason, M. Cooper, R. S. Holt, I. Bailey, and T. J. L. Jones, Philos. Mag. B **43**, 931 (1981).
[18]A. J. Rollason, R. S. Holt, and M. J. Cooper, Philos. Mag. B **47**, 51 (1983).
[19]N. Shiotani, Y. Tanaka, M. Ito, N. Sakai, Y. Sakurai, H. Sakurai, F. Itoh, T. Iwazumi, H. Kawata, and M. Ando, in *Positron Annihilation,* edited by Zs. Kajcsos and Cz. Szeles, Materials Science Forum Vol. 105-110 (Trans Tech, Switzerland, 1992), p. 833.
[20]N. Shiotani, T. Okada, T. Mizoguchi, and H. Sekizawa, J. Phys. Soc. Jpn. **38**, 423 (1975).
[21]A. K. Singh, A. A. Manuel, R. M. Singru, R. Sachot, E. Walker, P. Descouts, and M. Peter, J. Phys. F **15**, 2375 (1985).
[22]T. Kubota, H. Nakashima, H. Kondo, S. Tanigawa, Y. Murakami, Y. K. Cho, and G. W. Bahng, in *Positron Annihilation,* edited by Zs. Kajcsos and Cz. Szeles, Materials Science Forum Vol. 105-110 (Trans Tech, Switzerland, 1992), p. 723.
[23]N. Shiotani, N. Sakai, F. Itoh, M. Sakurai, H. Kawata, Y. Amemiya, and M. Ando, Nucl. Instrum. Methods Phys. Res. A **275**, 447 (1987).
[24]L. M. Pecora, J. Phys. Condens. Matter **SA1**, 1 (1989).
[25]P. E. Mijnarends, in *Positron Solid State Physics,* edited by W. Brandt and A. Dupasquier (North-Holland, Amsterdam, 1983), p. 146; P. E. Mijnarends, in *Positrons in Solids,* edited by P. Hautojärvi (Springer-Verlag, Heidelberg, 1979), p. 25.
[26]A. B. Migdal, Zh. Eksp. Teor. Fiz. **5**, 399 (1957) [Sov. Phys. JETP **5**, 333 (1957)].
[27]E. Daniel and S. H. Vosko, Phys. Rev. **120**, 2041 (1960).
[28]C. K. Majumdar, Phys. Rev. **140**, A227 (1965).
[29]D. A. Cardwell, M. J. Cooper, and S. Wakoh, J. Phys. Condens. Matter **1**, 541 (1989).
[30]D. A. Cardwell, Ph.D. thesis, University of Warwick, 1987.
[31]A. K. Singh, A. A. Manuel, T. Jarlborg, Y. Mathys, E. Walker, and M. Peter, Helv. Phys. Acta **59**, 410 (1986).
[32]S. Daniuk, G. Kontrym-Sznajd, J. Mayers, A. Rubaszek, H. Stachowiak, P. A. Walters, and R. N. West, J. Phys. F **17**, 1365 (1987).
[33]T. Jarlborg and A. K. Singh, Phys. Rev. B **36**, 4660 (1987).
[34]M. Matsumoto and S. Wakoh, J. Phys. Soc. Jpn. **56**, 3566 (1987).
[35]D. A. Cardwell and M. J. Cooper, J. Phys. Condens. Matter **1**, 9357 (1989).
[36]V. Sundararajan, D. G. Kanhere, and J. Callaway, Phys. Lett. A **133**, 521 (1988); V. Sundararajan, R. Asokamani, and D. G. Kanhere, Phys. Rev. B **38**, 12 653 (1988); V. Sundararajan and D. G. Kanhere, Pramana-J. Phys. **34**, 33 (1990); V. Sundararajan, D. G. Kanhere, and R. M. Singru, J. Phys. Condens. Matter **3**, 113 (1991).
[37]L. M. Pecora, A. C. Ehrlich, A. A. Manual, A. K. Singh, M. Peter, and R. M. Singru, Phys. Rev. B **37**, 6772 (1988).
[38]C. S. Wang and J. Callaway, Comput. Phys. Commun. **14**, 327 (1978); J. Callaway and C. S. Wang, Phys. Rev. B **16**, 2095 (1977).
[39]A. K. Rajagopal, S. P. Singhal, and J. Kimball (unpublished) as quoted by A. K. Rajagopal, in *Advances in Chemistry and Physics,* edited by G. I. Prigogine and S. A. Rice (Wiley, New York, 1979), Vol. 41, p. 59.
[40]A. K. Singh and R. M. Singru, J. Phys. F **12**, 685 (1982).
[41]N. Sakai, in *Positron Annihilation,* edited by Zs. Kajcsos and Cz. Szeles, Materials Science Forum Vol. 105-110 (Trans Tech, Switzerland, 1992), p. 431.
[42]G. P. Das, K. V. Bhagwat, and V. C. Sahni, Phys. Rev. A **36**, 2984 (1987).
[43]G. E. W. Bauer and J. R. Schneider, Z. Phys. B **54**, 17 (1983); G. E. W. Bauer and J. R. Schneider, Phys. Rev. B **31**, 681 (1985).
[44]A. J. Rollason, J. Schneider, D. Laundy, R. S. Holt, and M. J. Cooper, J. Phys. F. **17**, 1105 (1987).
[45]L. Lam and P. Platzman, Phys. Rev. B **9**, 5122 (1974).
[46]P. E. Mijnarends and R. M. Singru, Phys. Rev. B **19**, 6038 (1979).
[47]M. Sob, J. Phys. F **12**, 571 (1982).
[48]A. A. Manuel, Phys. Rev. Lett. **49**, 1525 (1982).
[49]D. G. Lock, V. H. C. Crisp, and R. N. West, J. Phys. F **3**, 561 (1973).
[50]A. K. Singh, A. A. Manuel, R. M. Singru, and M. Peter, Helv. Phys. Acta **58**, 640 (1985).